Journal of Alloys and Compounds 509 (2011) 7773–7777

Contents lists available at ScienceDirect

Journal of Alloys and Compounds

journal homepage: www.elsevier.com/locate/jallcom

Elaboration and dielectric study of ferroelectric or relaxor ceramics in the ternary system $BaTiO_3$–$NaNbO_3$–$BaSnO_3$

Abdelhedi Aydi[a,*], Annie Simon[b], Dominique Michau[b], Régnault Von Der Mühll[b], Najmeddine Abdelmoula[a], Hamadi Khemakhem[a]

[a] Laboratoire des Matériaux Ferroélectriques, Faculté des Sciences de Sfax, 3018 Sfax, Tunisia
[b] CNRS, Université de Bordeaux, ICMCB, 87 Avenue Dr A. Schweitzer, F-33608 Pessac, France

ARTICLE INFO

Article history:
Received 25 November 2010
Received in revised form 27 April 2011
Accepted 27 April 2011
Available online 10 May 2011

Keywords:
Ceramic
Permittivity
Ferroelectric
Relaxor
Polarisation
Stannate
Titanate
Raman
Piezoelectricity

ABSTRACT

The present work reports the elaboration and physical investigation of new compounds of the following composition $Ba_{1-x}Na_x(Ti_{1-y}Sn_y)_{1-x}Nb_xO_3$ (BTSnN*xy*). The studied ternary system presents some continuous solid solutions between the next 3 phases: the $NaNbO_3$ antiferroelectric phase that becomes easily ferroelectric at low rate substitutions, the $BaTiO_3$ ferroelectric phase and the paraelectric stannate phase $BaSnO_3$. Two different dielectric behaviors can be observed once some substitutions are made either in A or B sites of an ABO_3 perovskite. These substitutions modify the dielectric properties of the material. The introduction of Sn^{4+} and Ti^{4+} cations in the B site favors, respectively, a decrease of the transition temperature and an increase in the value of the real dielectric permittivity. The transition temperature should be modulated by varying the rate of cationic substitution. Some relaxor materials can be obtained at a temperature around room temperature.

1. Introduction

Stannates with the general formula $MSnO_3$, where M = Ca, Sr or Ba, are dielectric materials that can be used as thermally stable capacitors [1–4].

Sodium niobate $NaNbO_3$ is a dielectric material with a perovskite type structure. At room temperature, it crystallizes with orthorhombic symmetry (Pbma), shows antiferroelectric behavior, and becomes ferroelectric at high temperature (Curie temperature $T_C = 360\,^{\circ}C$) [5].

$BaTiO_3$ is an ABO_3 perovskite type with displacive ferroelectric properties. The substitution in the Ba or Ti sites with other ions or cations leads to remarkable changes in various characteristics [6,7].

In relaxor ferroelectric, there is an increase of T_m and a decrease of the real part of permittivity (ε'_r) with increasing frequency, where T_m is the temperature of the maximum dielectric permittivity. One broad peak with frequency dispersion takes place in real and imaginary parts of the maximum permittivity.

In the prototypical relaxor PMN ($PbMg_{1/3}Nb_{2/3}$), the disordered distribution of cations in the B site plays an important role in the classical non-relaxor–relaxor transition just like BTZ system [8–10]. The origin of the relaxor phenomenon is a dynamic polar cluster created by a disordered distribution of A and B site substitutions [11–15].

In the binary oxide system $[xNaNbO_3 + (1-x)BaSnO_3]$, single-phase perovskite compounds have already been obtained. When the composition x increases, the values of T_m, the dielectric permittivity at T_m, and ε'_{rmax} increase significantly [16,17].

Therefore, it is of great interest to investigate the correlation between substitution effect in the A and B sites and the role played by the introduction of Sn atoms on the modification of the chemical bonding in order to explain the dielectric properties of the solid solution BTSnN*xy*.

Developed were new ferroelectric or relaxor compounds ($Ba_{1-x}Na_x(Ti_{1-y}Sn_y)_{1-x}Nb_xO_3$) with high permittivity close to 300 K.

2. Experimental details

BTSnN*xy* ceramic samples with composition ($0.60 \leq x$ and $y \leq 0.75$) were elaborated by solid state reaction at 1030 °C for 15 h under an oxygenic atmosphere, using $BaCO_3$, Na_2CO_3, TiO_2, SnO_2, and Nb_2O_5 powders in stoichiometric amounts.

* Corresponding author.
E-mail addresses: aydi_abdelhedi@yahoo.fr (A. Aydi), simon@icmcb-bordeaux.cnrs.fr (A. Simon).

0925-8388/$ – see front matter © 2011 Elsevier B.V. All rights reserved.
doi:10.1016/j.jallcom.2011.04.149

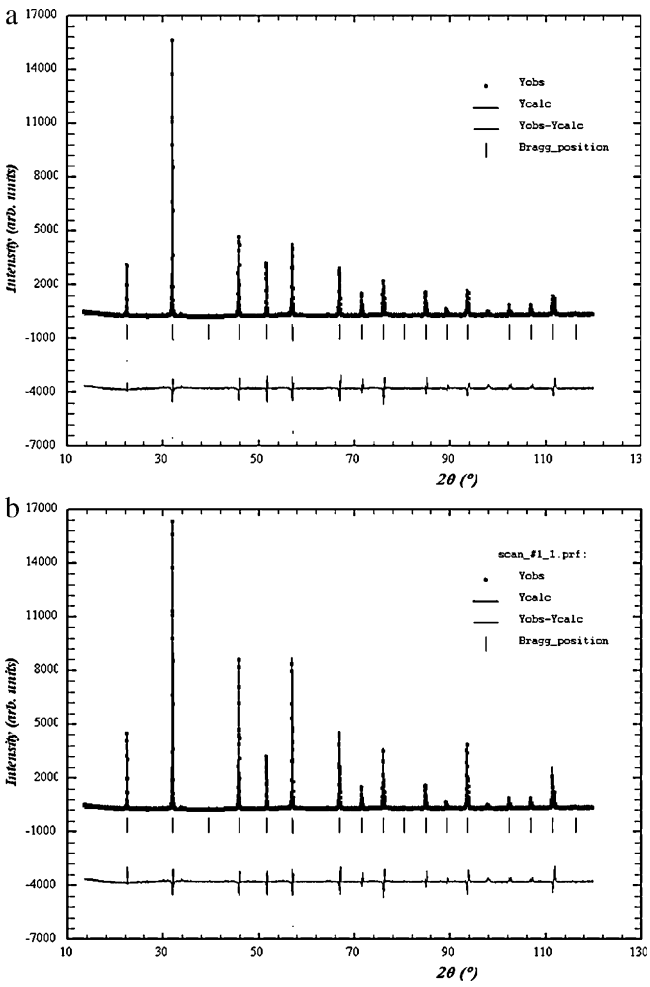

Fig. 1. (a) X-ray diffraction pattern of a BTSnN*xy* powder with composition corresponding to $x = 0.80$ and $y = 0.20$. (b) X-ray diffraction pattern of a BTSnN*xy* powder with composition corresponding to $x = 0.825$ and $y = 0.10$.

Powders were pressed under 100 MPa into disks of 8 mm in diameter and about 1 mm in thickness. Calcination at 1030 °C for 15 h was followed by 2 h of sintering at 1250 °C for $0.60 \leq x$ and $y \leq 0.75$. The diameter shrinkage, $\Delta\Phi/\Phi = (\Phi_{init} - \Phi_{end})/\Phi_{init}$, and the compactness (experimental density/theoretical density) were determined. Their average values were 12–15% and 92–94%, respectively, depending on the composition.

At room temperature, the powder was analyzed by X-ray diffraction patterns by means of a Philips Diffractometer, using the CuKα radiation, the angular range $10° \leq 2\theta \leq 110°$, and a 10 s interval for each step of 0.02°. This allows to determine the symmetry and the limits of the solid solution region at room temperature.

Dielectric measurements were performed on sintered ceramic disks (6.5 mm diameter and 1 mm thickness) after deposition of gold electrodes (600 nm min^{-1} for 10 min) on the circular faces by cathodic sputtering. The real and imaginary parts of relative permittivity ε'_r and ε''_r were determined under a Helium atmosphere as a function of both temperature (80–600 K) and frequency (10^2–2.10^6 Hz) using a Wayne-Kerr 6425 frequency analyzer.

Piezoelectric measurements were performed at 300 K using an impedance analyser (HP 4194 A).

A scanning microscope (SEM), JEOL 6360A, was used to characterize the microstructure.

The Raman spectra were recorded on a Horiba Lab-ram HR 800 instrument using the 633 nm exciting light of argon laser.

3. Results and discussion

The XRD patterns of BTSnN*xy* ($0.60 \leq x$ and $y \leq 0.75$) result in either a tetragonal or cubic structure at room temperature for all compounds. For example, patterns of BTSnN*xy* ($x = 0.80$ $y = 0.20$, and $x = 0.825$ $y = 0.10$) ceramics are shown in Fig. 1(a) and 1(b), respectively. The results reveal a single perovskite phase indicating that

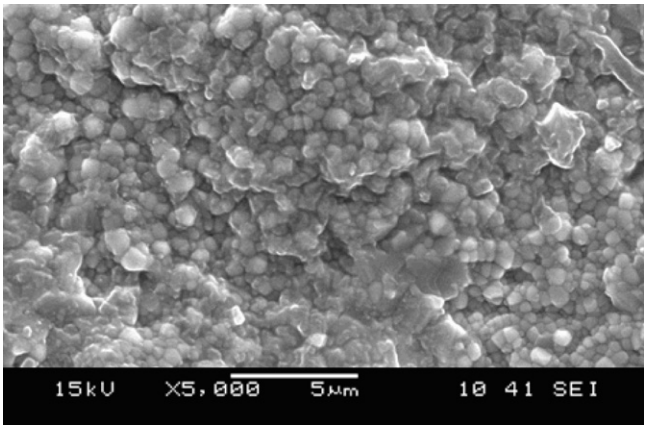

Fig. 2. SEM picture of the surface of a BTSnN*xy* ceramic ($x = 0.90$ and $y = 0.75$).

Ti^{4+} diffuses into the B-site of $Ba_{1-x}Na_x[Sn_{1-x}Nb_x]O_3$. The unit cell and profile parameters were determined using a global profile-matching method with the software "fullprof" [18]. The estimated value of unit cell parameters *a*, *c* and volume *V* are given in Table 1 of BTSnN*xy* ($x = 0.60, 0.70, 0.80, 0.825, 0.90$ and $y = 0.10, 0.20, 0.525, 0.75$). The symmetry of the ceramic specimens appears to be cubic with space group *Pm*3*m* or tetragonal *P*4*mm*. The decrease in the lattice parameters when *x* increases and *y* decreases can be due to the values of ionic radii *r* ($Na^+ = 1.18$ Å) and *r* ($Nb^{5+} = 0.64$ Å) for $NaNbO_3$ quite lower than those of *r* ($Ba^{2+} = 1.61$ Å), *r* ($Sn^{4+} = 0.69$ Å) and *r* ($Ti^{4+} = 61$ Å) for $Ba(Sn,Ti)O_3$.

The SEM micrograph of BTSnN ($x = 0.9, y = 0.75$) ceramic is shown in Fig. 2. All samples were sintered at 1250 °C for 2 h. A well-dense ceramic is obtained with an average grain size of the order of 2 μm for all compounds BTSnN ($x = 0.60, 0.70, 0.80, 0.825, 0.90$ and $y = 0.10, 0.20, 0.525, 0.75$).

The temperature dependence of the real ε'_r and imaginary ε''_r parts of the permittivity in the frequency range 0.1–200 kHz for BTSnN*xy* is shown in Fig. 3. As examples, classical ferroelectric (Fig. 3(a)), relaxor (Fig. 3(b)), relaxor at T_m near 300 K (Fig. 3(c)) and the imaginary part of the permittivity (Fig. 3(d)) are noted. Three anomalies are observed on heating, for compositions close to $BaTiO_3$, i.e. the solid solution BTSnN*xy* ($x = 0.90$, $y = 0.10$). These anomalies are related to phase transitions: trigonal-orthorhombic at T_2, orthorhombic-tetragonal at T_1 and tetragonal-cubic at T_C. The values of $T_C = 468$ K, $T_1 = 240$ K and $T_2 = 320$ K, were independent from frequency. For $BaTiO_3$, these temperatures have been observed at $T_C = 393$ K, $T_1 = 268$ K and $T_2 = 183$ K [19,20]. For the relaxor compounds like BTSnN*xy* ($x = 0.60$, $y = 0.10$), we only observe the relaxor/paraelectric transition at T_m. T_m is near 300 K for some compositions (BTSnN*xy*: $x \geq 0.80$, $y \leq 0.20$).

Depending on the composition, two types of behavior appear: classical ferroelectric or relaxor. Fig. 4 shows the ternary diagram $BaTiO_3$–$NaNbO_3$–$BaSnO_3$. When the rate y of Sn^{4+} substitution increases, T_C (tetragonal-cubic) decreases strongly (Fig. 5) as for the BSnN0.9 solid solution [16]. When the Ti^{4+} ratio increases, ε'_{rmax} increases exponentially (Fig. 6).

The admittance and susceptance of a sintered cylindrical ceramic disk (6.5 mm in diameter and 0.6 mm thickness) with composition BTSnN*xy* ($x = 0.825$, $y = 0.10$) were measured versus frequency around the main transverse resonance mode. The ceramic is polarized under continuous field of 1.6 kV at 300 K for 15 min. The variation of the admittance (*G*) and the susceptance (*B*) versus frequency is reported in Fig. 7. The calculation of the transverse piezoelectric coefficient at room temperature gives $d_{31} = -1.695$ pC/N.

Table 1
Refined unit cell parameters for BTSnN*xy* ceramics ($x = 0.60, 0.70, 0.80, 0.825, 0.90$ and $y = 0.10, 0.20, 0.525, 0.75$).

x	$y = 0.1$			$y = 0.2$			$y = 0.525$			$y = 0.75$		
	a (Å)	c (Å)	V (Å^3)	a (Å)	c (Å)	V (Å^3)	a (Å)	c (Å)	V (Å^3)	a (Å)	c (Å)	V (Å^3)
0.6	3.978		62.949	4.031		65.499	4.052		66.528			
0.7	3.965		62.334	4.022		65.061	4.041		65.988	4.054		66.627
0.8	3.957		61.958	4.01		64.481	4.033		65.597	4.042		66.037
0.825	3.954	3.968	62.036	4.008	4.018	64.545	4.031	4.044	65.710			
0.9	3.948	3.971	61.894	4.000	4.024	64.384	4.028	4.035	65.467	4.039	4.042	65.939

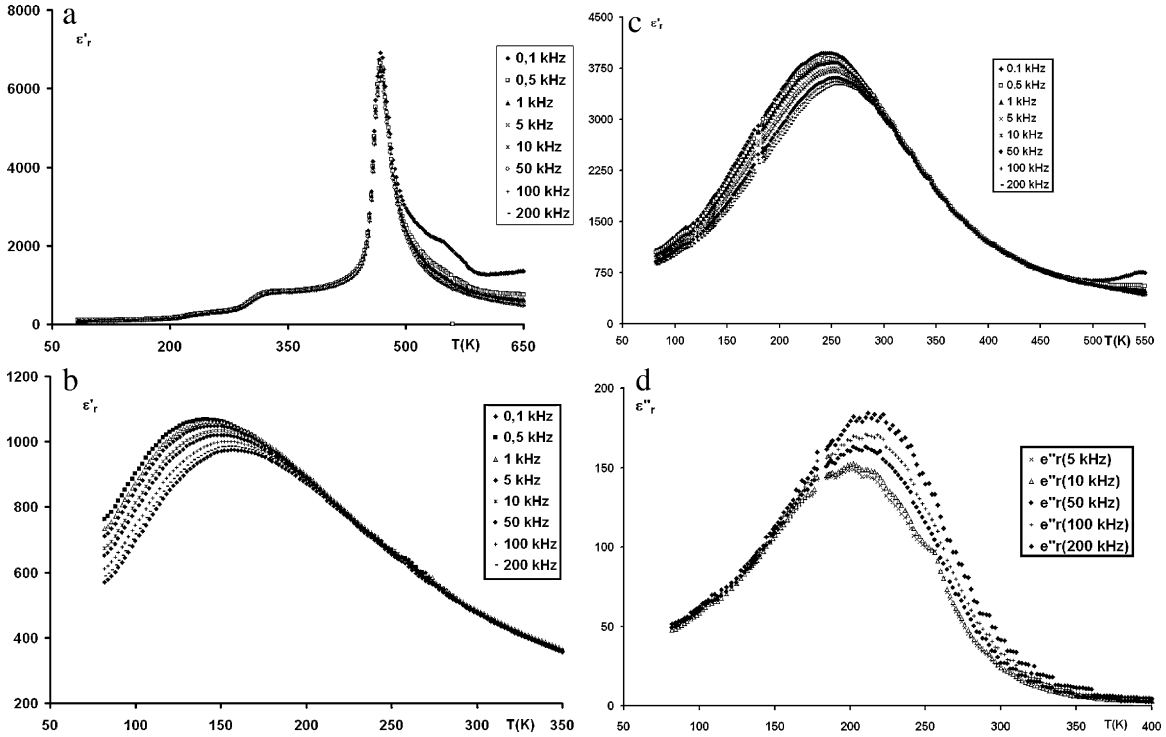

Fig. 3. (a) Thermal variation of permittivity ε'_r for a ceramic sample BTSnN*xy* with composition corresponding to $x = 0.90$ and $y = 0.10$. (b) Thermal variation of permittivity ε'_r for a ceramic sample BTSnN*xy* with composition corresponding to $x = 0.60$ and $y = 0.10$. (c) Thermal variation of permittivity ε'_r for a ceramic sample BTSnN*xy* with composition corresponding to $x = 0.80$ and $y = 0.20$. (d) Thermal variation of permittivity ε''_r for a ceramic sample BTSnN*xy* with composition corresponding to $x = 0.80$ and $y = 0.20$.

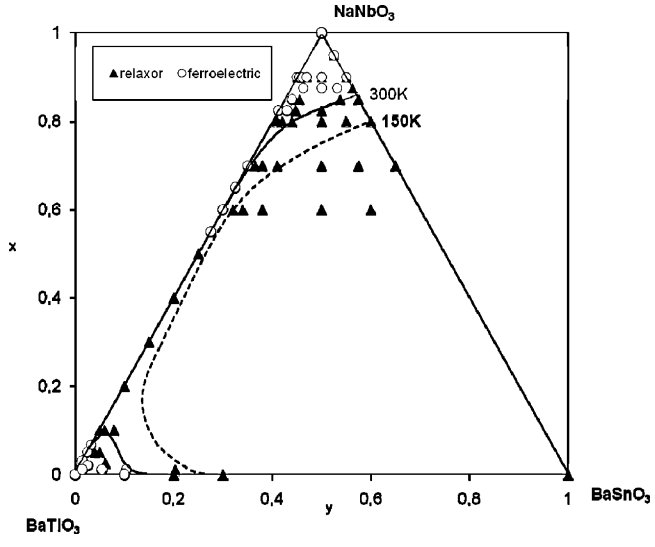

Fig. 4. Relaxor and ferroelectric phases in the ternary diagram $BaTiO_3$–$NaNbO_3$–$BaSnO_3$.

Fig. 8 depicts the room temperature spectra for 4 compositions of the solid solutions BTSnN*xy* ($x = 0.8$, $y = 0.1$), ($x = 0.90$, $y = 0.20$), ($x = 0.7$, $y = 0.5$) and ($x = 0.85$, $y = 0.75$) (in the wave number range 50–1500 cm^{-1}). Raman spectra show vibration bands which weaken and broaden with increasing content of $BaTiO_3$ due to the presence of disorder in the cubic phase [21]. This disorder stems

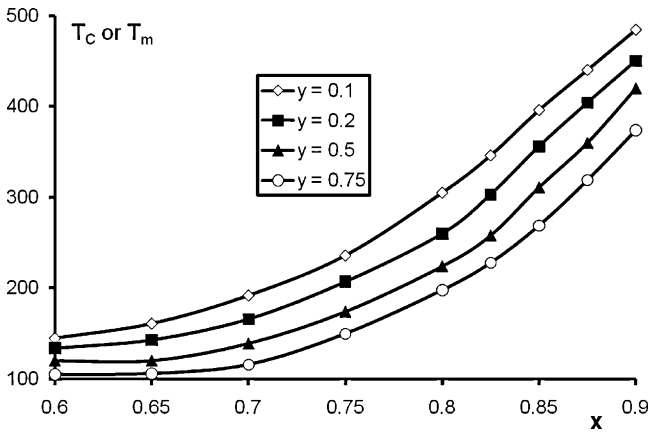

Fig. 5. Variation of T_C or T_m vs. composition for BTSnN*xy* ceramics.

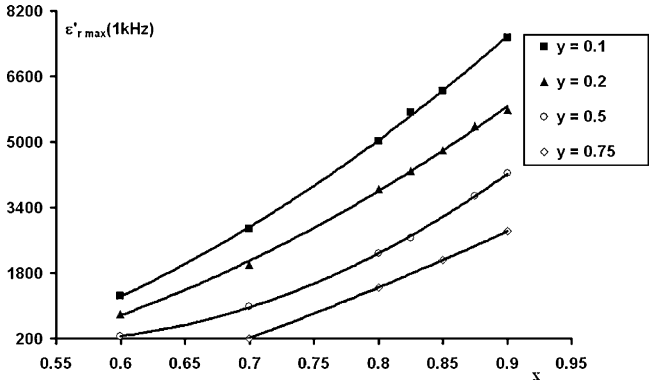

Fig. 6. Variation of ε'_{rmax} (1 kHz) vs. composition for BTSnN*xy* ceramics.

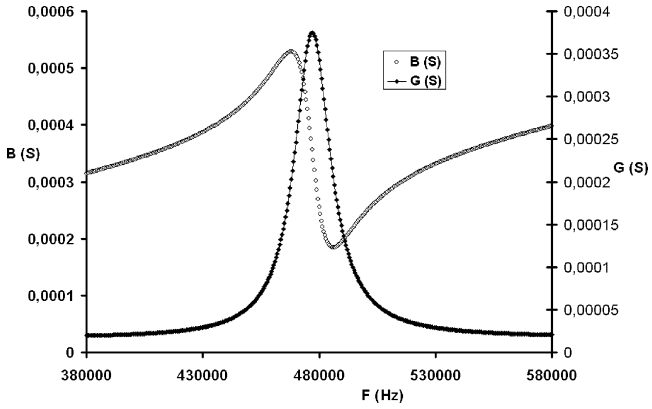

Fig. 7. Variation of the admittance (G) and the susceptance (B) as functions of frequency at T = 300 K for BTSnN*xy* ceramic with x = 0.825 and y = 0.10.

from the displacement of Sn/Ti/Nb cations along the cubic diagonals [22]. These modes appear at frequencies close to those of $BaTiO_3$ and $NaNbO_3$ [23].

The cubic perovskite structure with O_h symmetry above T_C distorts into a tetragonal structure C_{4V} [24,25]. Using a standard group theory analysis, normal optic modes can be shown to belong to the $3T_{1u} \oplus T_{2u}$ irreducible representations of the point group O_h. When entering the tetragonal C_{4v} symmetry, the IR active T_{1u} modes are expected to split into $A_1 \oplus E$, and the silent mode T_{2u} into $B_1 \oplus E$ [26,27]. The peak attributed to the Nb–O phonon is observed in Raman spectrum at 203 and 553 cm^{-1} for BTSnN*xy* (x = 0.80, y = 0.10), at 313 and 807 cm^{-1} for BTSnN*xy* (x = 0.90, y = 0.20), at 205 and 563 cm^{-1} for BTSnN*xy* (x = 0.70, y = 0.50) and at 236 and 614 cm^{-1} for BTSnN*xy* (x = 0.85, y = 0.75). The peak attributed to Sn–O is observed at 824, 842, 876 and 1160 cm^{-1} for BTSnN*xy* (x = 0.8, y = 0.1), (x = 0.7, y = 0.5), (x = 0.85, y = 0.75) and (x = 0.90, y = 0.20), respectively. All the bands were accompanied by a significant broadening, a weaker intensity and a shift toward the high frequencies. The dynamic of the structure was studied by analyzing the characteristic modes associated with nano-regions in relaxors. This deduction is based on the fact that local symmetry of nano-regions is different from that of the global symmetry.

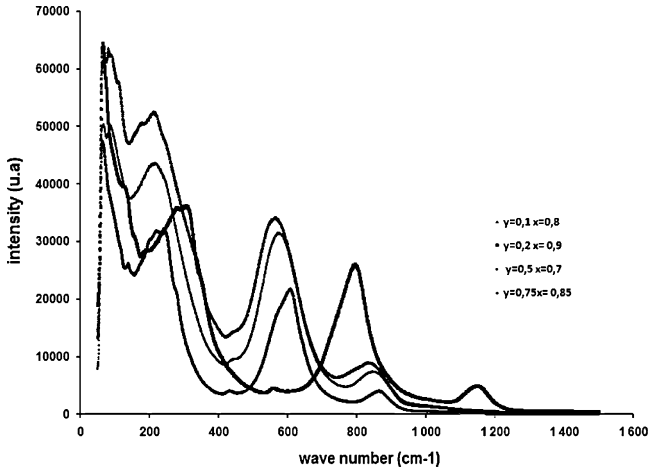

Fig. 8. Raman spectra of BTSnN*xy* ((y = 0.1, x = 0.8), (y = 0.20, x = 0.90), (y = 0.5, x = 0.7) and (x = 0.85, y = 0.75)) ceramics at room temperature.

4. Conclusions

New BTSnN*xy* ceramics have been elaborated by a solid-state technique. The dielectric permittivity was systematically studied. Structural and piezoelectric measurements and Raman spectroscopy analysis were carried out on selected compositions to complement the understanding of the materials' behavior. The results of XRD show that Ti^{4+} diffuses into the $Ba_{1-x}Na_xSn_{1-}xNbxO_3$ (BSnN*x*) lattice to form a solid solution with a perovskite type phase of the composition $Ba_{1-x}Na_x(Ti_{1-y}Sn_y)_{1-x}Nb_xO_3$ (BTSnN*xy*) in the range $0.60 \leq x$ and $y \leq 0.75$.

Dielectric measurements show two kinds of behavior depending on the composition: classical ferroelectric or relaxor types. The relaxor effect is due to a modification of the chemical bonding that results in the substitution of Ti for Sn. As it has been already reported, the screen effect due to internal *d* electrons of Sn atoms decreases the polarization coupling in the ferroelectric lattice. Thus, the disorder is between Sn and Ti.

The studies of the dielectric properties of the composition show that in the $NaNbO_3$–$MSnO_3$ (M = Ba, Ca) solid solutions, the origin of the relaxor effect is due to the introduction of Sn^{4+} in octahedral site.

For low $NaNbO_3$ substitution rates, the crystalline network has Nb–O bonds in which the covalent character allows long-distance cooperative interactions that involve the ferroelectric character.

The increase in the amount of Tin in the network causes many ionic Sn–O links. They break the cooperative effect of Nb–O bonds. It appears nano-domains of Nb–O clusters, isolated from one another by Sn–O links which give the relaxor behavior. Electron density theoretical studies have shown that Sn–O bonds were more delocalized than Nb–O ones. The delocalization of the electronic cloud should be explained by the screen effect of internal 3D electrons of the tin atoms.

Compared with the pure BSnN*x* compounds, the BTSnN*xy* ceramics exhibit an increase in ε'_{rmax} and a decrease in T_m or T_C by addition of $Ti^{4+}$and Sn^{4+}, respectively.

The variation in the large chemical composition of these ceramics allows a possible control of their physical properties.

References

[1] B. Jaffe, W.R. Cook Jr., H. Jaffe, Piezoelectric Ceramics, Academic, New York, 1986, p. 121.
[2] R. Buchanan, Ceramic Materials for Electronic Applications, Dekker, New York, 1986, p. 69.
[3] X.Y. Ch, M. Chao, B. Shi Ping, Z. Hai Yan, J. Alloys Compd. 497 (2010) 354.
[4] A.S. Deepa, S. Vidya, P.C. Manu, S. Solomon, A. John, J.K. Thomas, J. Alloys Compd. 509 (2011) 1830.
[5] H.D. Megaw, Ferroelectrics 7 (1974) 87.
[6] S. Komine, E. Iguchi, J. Phys.: Condens. Matter 14 (2002) 2043.
[7] S.K. Jo, J.S. Park, Y.H. Han, J. Alloys Compd. 501 (2010) 259.
[8] A. Simon, J. Ravez, Solid. State Sci. 7 (2005) 925.
[9] V.A. Isupov, Ferroelectrics 90 (1989) 113.
[10] C. Malibert, et al., J. Phys.: Condens. Matter 9 (1997) 7485.
[11] V. Westphal, W. Kleemann, M.D. Glinchuk, Phys. Rev Lett. 68 (1992) 847.
[12] L.E. Cross, Ferroelectrics 76 (1987) 241.

[13] J. Ravez, C. Broustera, A. Simon, J. Mater. Chem. 9 (1999) 1609.
[14] P. Sciau, G. Calvarin, J. Ravez, Solid. State Commun. 113 (1999) 77.
[15] S.A. Prosandeev, et al., J. Phys.: Condens. Matter 13 (2001) 5957.
[16] A. Aydi, H. Khemakhem, C. Boudaya, R. Von Der Mühll, A. Simon, Solid. State Sci. 6 (2004) 333.
[17] H. Khemakhem, A. Simon, R. Von Der Mühll, J. Ravez, J. Phys.: Condens. Matter 12 (2000) 5951.
[18] J. Rodriguez-Carvajal. Program FullProf, Laboratoire Léon Brillouin (CEA-CNRS) Version 3.5d – LLB – JRC, October 1998.
[19] L. Khemakhem, A. Kabadou, A. Maalej, A. Ben Salah, A. Simon, M. Maglione, J. Alloys Compd. 452 (2008) 451.
[20] N. Nanakorn, P. Jalupoom, N. Vaneesorn, A. Thanaboonsombut, J. Ceram. Int. 34 (2008) 779.
[21] L.-M. Li, Y.-J. Jiang, L.-Z. Zeng, J. Raman Spectrosc. 27 (1996) 503.
[22] R. Comes, M. Lambert, A. Guinier, Solid State. Commun. 6 (1968) 715.
[23] F. Bahri, A. Simon, H. Khemakhem, J. Ravez, J. Phys. Stat. Sol. (a) 184 (2001) 459.
[24] A. Aydi, H. Khemakhem, A. Simon, D. Michau, R. Von Der Mühll, J. Alloys Compd. 484 (2009) 356.
[25] A. Aydi, H. Khemakhem, C. Boudaya, R. Von Der Mühll, A. Simon, Solid. State Sci. 7 (2005) 249.
[26] R. Farhi, M. El Marssi, A. Simon, J. Ravez, Eur. Phys J. B 9 (1999) 599.
[27] N. Baskaran, H. Chang, Mater. Chem. Phys. 77 (2003) 889.